

ASTROPHYSICS AND GRAVITY DIVISION

Overview

Astrophysics and Gravity Division consists of Gravitational Wave Group, The Observational Cosmology Group, Primary Cosmic Ray Group and Theory Group.

The Gravitational Wave Group conducts experimental research of gravitational wave with researchers of gravitational wave experiment and theory in Japan. The main items are the construction of the large scale cryogenic interferometer(KAGRA) at Kamioka underground and the operation of CLIO. For this purpose, KAGRA observatory was established at the beginning of the fiscal year of 2016 to assist the construction of KAGRA gravitational wave telescope.

The Observational Cosmology Group studies the cosmic history based on deep multi-wavelength observations in collaboration with worldwide researchers. This group has started a new optical deep survey project with the wide-field imager of Hyper Suprime-Cam mounted on the Subaru telescope.

Theory Group conducts both theoretical study of the Universe and astroparticle physics.

Gravitational Wave Group

KAGRA Project Status

[Spokesperson : Takashi UCHIYAMA]

ICRR, The Univ. of Tokyo, Hida, Gifu 506-1205

Overview

KAGRA, Large-scale Cryogenic Gravitational wave Telescope, aims at detecting gravitational waves and developing gravitational wave astronomy, which was established by the first detection of gravitational waves by LIGO. KAGRA employs a 3 km L-shaped laser interferometer with a cryogenic mirror system placed underground at Kamioka[1]. The KAGRA development is divided into two stages: the initial KAGRA (iKAGRA) and baseline KAGRA (bKAGRA). The iKAGRA interferometer is a simple Michelson interferometer with a 2-Watt laser, room-temperature mirrors, and a simple vibration isolation system. We completed the iKAGRA interferometer with a test run in April 2016[2]. Then we proceeded to bKAGRA.

Figure 1 and 2 show a schematic view of optical layout of the bKAGRA interferometer and the KAGRA vibration isolation systems. Table 1 shows design parameter of the bKAGRA interferometer[4]. The bKAGRA interferometer will employ a Resonant Sideband Extraction (RSE) interferometer with 180-Watt laser, cryogenic Sapphire mirrors, and several kinds of vibration isolation systems. The bKAGRA interferometer should attain the sensitivity high enough for the detection of gravitational waves with the help of the high power

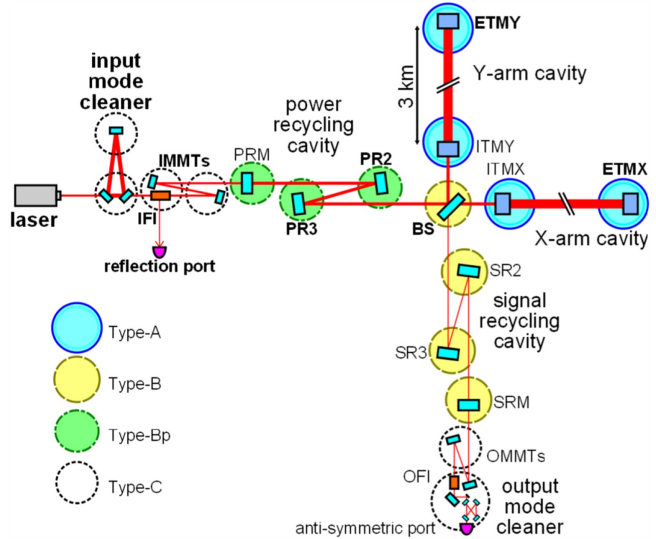


Fig. 1. Schematic view of the bKAGRA interferometer[4]. Type-A, Type-B, Type-Bp, and Type-C are the names of vibration isolation system for each mirror.

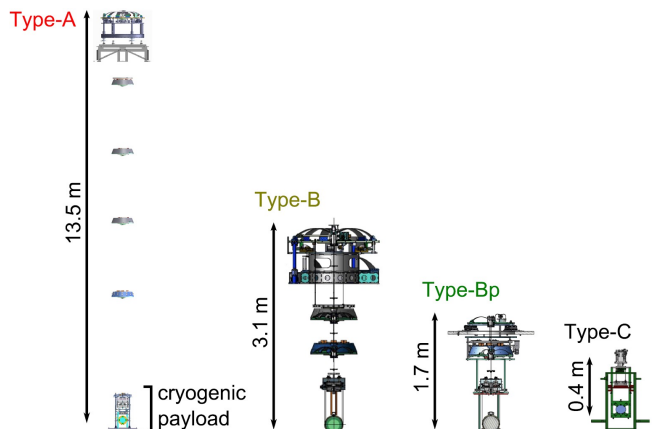


Fig. 2. KAGRA vibration isolation systems[4]. KAGRA equips four kinds of vibration isolation systems such as Type-A, Type-B, Type-Bp, and Type-C.

laser and RSE interferometer to reduce the quantum noise, the cryogenic Sapphire mirrors to reduce the thermal noise, and the vibration isolation systems to reduce the seismic noise. Figure 3 shows designed sensitivities of bKAGRA in case of Broadband RSE (BRSE) and of Detuned RSE (DRSE), where incoherent sum of the fundamental noise sources is assumed. Observation range for an in-spiral and merger of neutron-star binary reaches 135 Mpc in BRSE and 153 Mpc in DRSE with the same definition of the observation range as LIGO and Virgo.

Figure 4 shows the international collaborative observation scenario[3]. LIGO conducted Observation 1 (O1) from

Table 1. The design parameters of the bKAGRA interferometer[4].

Arm cavity length	3000 m	Test mass size	$\phi 22\text{ cm} \times 15\text{ cm}$
Laser wave length	1064 nm	Mass of test mass	22.8 kg
Input power at PRM	67W	Temperature of test mass	22 K
Arm intra-cavity power	340 kW	Beam radius at test mass	3.5 cm
ITM transmittance	0.4 %	PRC/SRC lengths	66.6 m
PRM transmittance	10 %	Detuning angle	3.5 deg
SRM transmittance	15 %	Homodyne angle	135.1 deg

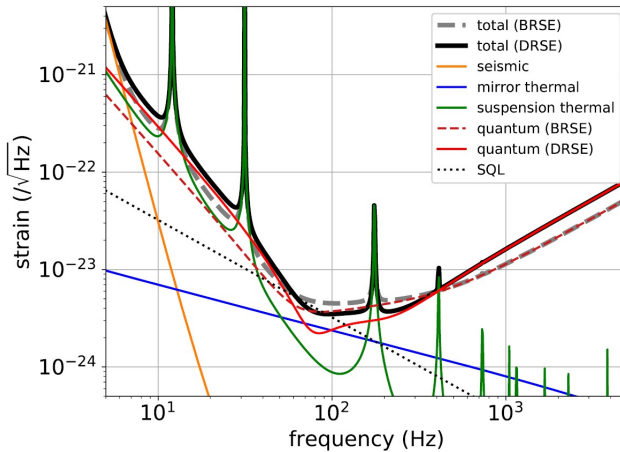


Fig. 3. The designed sensitivity of the bKAGRA interferometer[4]. "total", "seismic", "mirror thermal", "suspension thermal", "quantum", and "SQL" mean total sum of fundamental noise sources shown in this figure, seismic noise including gravity gradient noise, mirror thermal noise, suspension thermal noise, quantum noise, and standard quantum limit, respectively. The figure shows "total" and "quantum noise" in both Broadband RSE (BRSE) and Detuned RSE (DRSE) case. Observation range for an in-spiral and merger of neutron-star binary reaches 135 Mpc in BRSE and 153 Mpc in DRSE with the same definition of the observation range as LIGO and Virgo.

September 12th, 2015 to January 19th, 2016 and Observation 2 (O2) from November 30th, 2016 to August 25th, 2017. Virgo joined O2 from August 1st, 2017. LIGO and Virgo started Observation 3 (O3) from April 1st, 2019 and O3 will continue by the end of April in 2020. KAGRA is aiming to join O3 in 2019.

In FY2018 we started with an operation of KAGRA interferometer as bKAGRA phase 1 which is 3 km Michelson interferometer with two sapphire mirrors suspended by the Type-A vibration isolation systems. One sapphire mirror was cooled at 18 K. The operation was done from April 28 to May 6 in 2018 and it was the first demonstration of operating km-class interferometer at cryogenic temperature. Figure 5 and Figure 6 shows a summary of daily status of the operation and a strain sensitivity comparing with noise sources[4], respectively. Duty factor in the first half of the operation reached 88.6%. The observation range for an in-spiral and merger of neutron-star binary and BH binary reached 17 pc and 100 pc, respectively. The longest continuous operation time was 11.1 hour.

After the bKAGRA phase 1 operation, we started con-

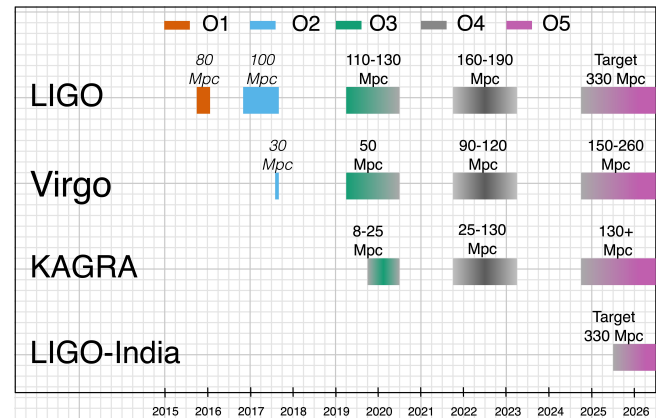


Fig. 4. International observation scenario[3]. Virgo was joined in Observation 2 (O2) from August 1st in 2017. LIGO and Virgo started Observation 3 (O3) from April 1st in 2019. O3 will continue by the end of April in 2020. KAGRA is aiming to join O3 in 2019.

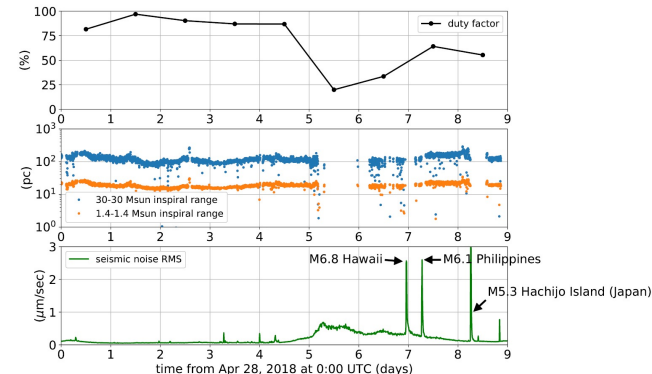


Fig. 5. Daily status of bKAGRA phase 1 operation[4]. The figure shows daily duty factor (Top panel), inspiral range (Middle panel), and seismic noise level (Bottom panel) during the operation. The operation was done from April 28 to May 6 in 2018.

struction of the bKAGRA interferometer with 40 W laser power. What we have installed were an infrared laser system with the maximum power of 40 W, two sets of arm length stabilization system using a green laser, calibration systems using photon radiation pressure, large beam baffles, transmission monitor systems, some optics consisting a signal recycling cavity and output optics, two input test masses called ITMX and ITMY in Figure 1, and so on. Physical Environmental Monitor (PEM) is a sensor network consisting several kinds of environmental sensors such as accelerometers,

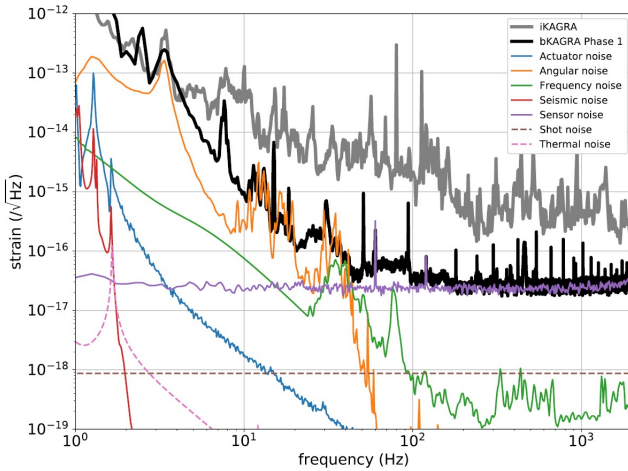


Fig. 6. Strain sensitivity of KAGRA in phase 1 operation[4].

seismometers, magnetometers, thermometers, acoustic sound monitors, power monitors and so on. Purpose of PEM is to check the detector health, noise sources, and data quality in cooperation with the detector characterization group. We placed many sensors in the KAGRA site and monitoring has already started.

We have tried lock acquisition of the X-arm cavity for the first time in parallel with the installation works mentioned above. The lock acquisition of the X-arm cavity was successfully achieved with helps of the arm length stabilization system. Then we carried out characterization of the X-arm cavity. Table2 shows a summary of optical parameters of the X-arm cavity comparing with designed and measured values.

We also enhanced the international collaborations with the Einstein Telescope (ET) project, LIGO, Virgo, Korean and other Asian groups mainly based on the JSPS core-to-core program.

The rapidly progressing status of KAGRA were presented in many international conferences. Many papers about the progress of KAGRA were also published [1], [4], [5]. We also presented activities on our web-page.[6]

Bibliography

- [1] "KAGRA: 2.5 generation interferometric gravitational wave detector", KAGRA collaboration, Nature Astronomy, Vol. 3, January 2019, 35-40
- [2] "Construction of KAGRA: an underground gravitational-wave observatory", KAGRA collaboration, Prog. Theor. Exp. Phys. 2018, 013F01 (2018)
- [3] "Prospects for observing and localizing gravitational-wave transients with Advanced LIGO, Advanced Virgo and KAGRA", Abbott, B.P., Abbott, R., Abbott, T.D. et al. arXiv:1304.0670v9 [gr-qc]
- [4] "First cryogenic test operation of underground km-scale gravitational-wave observatory KAGRA", KAGRA collaboration, Class. Quantum Grav. 36 165008 (2019)

[5] "An arm length stabilization system for KAGRA and future gravitational-wave detectors", KAGRA collaboration, to be published in Class. Quantum Grav. (2019)

[6] <http://gwcenter.icrr.u-tokyo.ac.jp/en/>

Vacuum system for KAGRA

[Spokesperson : Takashi UCHIYAMA]

ICRR, The Univ. of Tokyo, Hida, Gifu 506-1205

We firstly pumped six vacuum chambers those are IFI, IMM, PRM, PR3, PR2, and BS and vacuum pressure achieved order of 10^{-5} Pa. We made control boxes for seven large gate valves those are GVmc between MCF and IFI, GVbsx between BS and IXC, GVitm between IXA and the X-arm tube, GVitm between the X-arm and EXA, GVbsy between BS and IYC, GVitm between IYA and the Y-arm tube, and GVitm between the Y-arm and EYA. The control boxes has open/close control buttons and indicators. The GVs will be controlled by remotely via KAGRA machine control system which has Programable Logic Circuits through the control boxes.

Input and Output Optics

[Spokesperson : Keiko KOKEYAMA]

ICRR, The Univ. of Tokyo, Hida, Gifu 506-1205

The input and output optics of KAGRA consists of the pre-stabilization system for the laser, auxiliary locking system, input optics chain, output optics chain. The pre-stabilization system includes the frequency stabilization system, intensity stabilization system, pre-mode cleaner, and modulation system for the main interferometer. The auxiliary locking system includes the phase locking system for the green beam each for X and Y arms, the fiber system, and the locking system for the arm cavities. The input optics chain includes the input mode cleaner, input Faraday isolator, and two input mode matching telescopes. The output optics chain includes the output mode matching telescopes, output Faraday isolator, and output mode cleaner.

In the fiscal year of 2019, installations and commissioning works of most remaining systems have completed towards joining the O3 observation, as described below.

One of the major milestones in 2019 was the installation of the output optics chain. Three mirrors suspended by the type-C suspensions (double suspensions), output Faraday isolator, and output mode cleaner were installed. The three suspended mirrors are located downstream of the signal recycling mirror. The first two mirrors are the output mode matching telescopes (curved mirrors) and the third one is a steering mirror to steer the light to the output mode cleaner. The suspensions were developed by a collaboration with National Astronomical Observatory of Japan. The output Faraday isolator and output mode cleaner were developed and delivered from Tokyo Institute of Technology, and they were installed in the OMC chamber. After the installation of the output mode cleaner, the finesse of the cavity was found to be around 300, much

Table 2. Optical parameters of the X-arm cavity[5].

Parameter name	Designed	Measured
Cavity length	3000 m	29999.990(2) m
Finesse for 1064 nm	1530	1410(30)
Roundtrip loss for 1064 nm	< 100 ppm	86(3) ppm
Finesse for 532 nm	49.2	41.0(3)

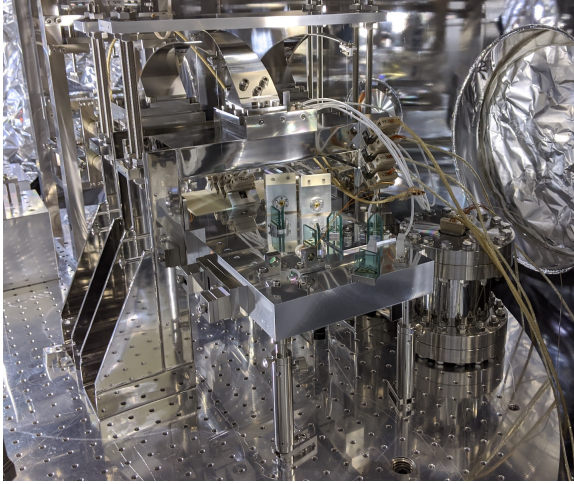


Fig. 7. The output mode cleaner installed in the vacuum chamber.

lower than the designed value of about 700. By our investigations on an in-air optical bench, one of the four mirrors of the output mode cleaner was found to be glued on the wrong side of the mirror wedge. Due to the tilted mirror, the cavity eigenmode was off from the ideal beam axis, and a beam spot on each mirror was off from its center. Although the exact reason of the lower finesse was not clearly identified, this can be one reason. To fix the wrong eigenmode, the mirror was swapped with a spare one and glued at the right angle. After changing the mirror, the measured finesse was confirmed as high as the design value in the air test bench. However, the finesse measured in the vacuum chamber after the re-installation was 580. The cause was not identified. Fig. 7 shows the photo of the output mode cleaner installed in the vacuum chamber.

For the input optics chain, by 2019, most of the important components had already installed and commissioned. The target in 2019 was to improve the high power compatibility. A beam shutter which can handle a high power beam was manufactured and installed in the pre-stabilized laser room. The shutter is custom made based on one used in Advanced LIGO. It is high-power compatible, and remotely controllable from the KAGRA control systems. The shutter consists of a steering mirror attached on a solenoid which can rotate 45 degrees so that the beam can be steered to the direction at 90 degrees to where a commercial high power beam dump with a water cooling system is placed. The installed shutter was found to fluctuate the beam by heat caused at the shutter's solenoid, as currents are applied on the solenoid when the shutter is open. We temporarily circumvented the issue by swapping the solenoid to another one whose rotation direction is opposite.

The solenoid's initial angle is also 45 degrees rotated compared with the original one so that it opens when currents are not applied therefore when the solenoid is not heated. However, from a safety point of view, the shutter must close when the current is not applied. The shutter has to be modified so in the near future.

The input mode cleaner which has been working since the iKAGRA phase was tested with a high power for the first time. The transmission power of 20 watts was achieved for about 50 minutes without observing any thermal problems such as thermal lensing effects.

A high power beam dump was specially designed, manufactured, and installed in the IFI chamber with a team from National Astronomical Observatory of Japan. It is to dump a high power beam, directly reflected light from the power recycling mirror (PRM), which is 90% of the incident beam. During initial alignment procedures and lock acquisition sequences, the PRM is misaligned intentionally not to flash the power recycling cavity. In such phases, the beam reflected by the misaligned PRM must be properly dumped not to damage any optics or suspension parts around it or not to significant scattered lights. The beam dump must be vacuum compatible and to be able to conduct the heat to outside of the vacuum enclosure. The beam dump consists of a V-shape structure made from silicon carbide (SiC) plates. The SiC plates are tightly fixed against copper holder parts with small Poly Ether Ether Ketone (PEEK) plates. The upper half of the structure is made of also copper to have high thermal conductivity whereas the lower half of the structure is a pedestal post made of SUS which has a smaller thermal conductivity compared with copper so not to heat up the optical table under the pedestal. Ten copper heat sinks are used to release the heat to the outside of the flange. The sinks are bolted to the copper part on one side, and the other side is linked to the vacuum flange of an OFC (oxygen-free-copper) disk of 230 mm in diameter and 20 mm thick, so that a heat is conducted and released to the atmosphere. A platinum thermal probe is attached on the top of the V-shape part so that the temperature of the beam dump can be monitored. The overall picture is depicted in Fig. 8. By the high power test of the input mode cleaner mentioned in the previous paragraph, the heat flow of the dump was also tested. As a result, we found that the heat flow needs to be modified. The temperature of the dump did not raise as expected, which suggests the majority of the heat was conducted by the SUS pedestal to the table.

In addition to the development of the high power beam dump, to protect the suspension fibers from exposures by the high power beam, solblack coated (light absorbing material by Asahi precision Co. Ltd.) metal plates were attached on the type-C suspensions of input mode-matching telescopes in

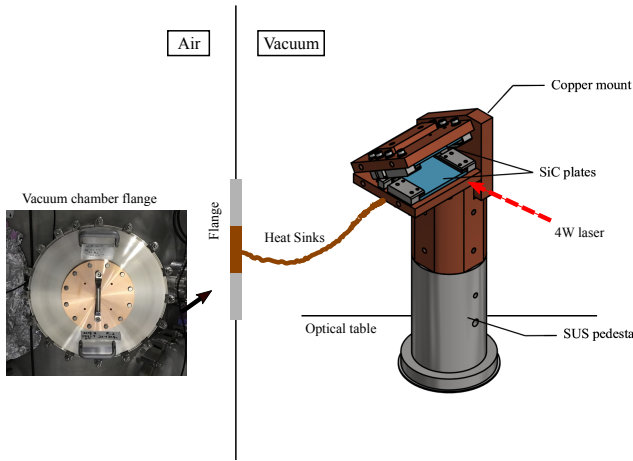


Fig. 8. The overall picture of the high power beam dump including the heat conduction path.

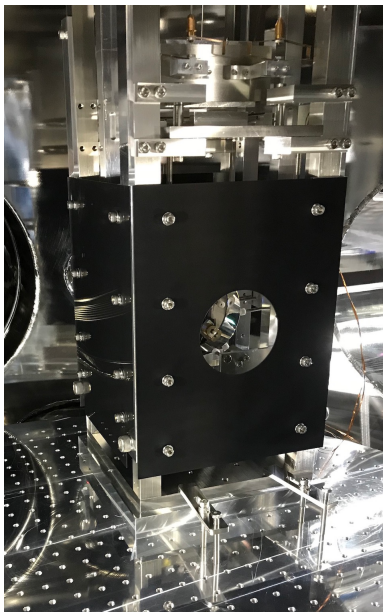


Fig. 9. Solblack coated shields were installed on input mode-matching telescopes to protect from direct exposures of high power laser beam.

the IFI and IMM chambers, as shown in Fig. 9.

In parallel of the experiments mentioned above, a proof-of-principle experiment for the Mach-Zehnder Modulation system (MZM) was successfully conducted. In the final phase of the KAGRA operation, aiming the quantum noise demolition, the signal recycling cavity will be detuned to produce optical springs. At the detuning phase, the signal recycling cavity is known to introduce great excess noise, a new modulation scheme to relax the noise coupling was proposed [1]. The new modulation system is with two Mach-Zehnder interferometer in series (MZM), and can apply both phase and amplitude modulations at an arbitrary ratio between them, by applying a phase difference between the oscillator signals on the corresponding two electro-optic modulators. Our proof-of-principle experiment successfully verified the new feature

of variable ratio between the phase and amplitude modulations. It was done as a topic of a master thesis of an ICRR student. The result was published in [2].

Cryogenic system

[Spokesperson : Takafumi USHIBA]
ICRR, The Univ. of Tokyo, Hida, Gifu 506-1205

One of unique features of KAGRA is cooling sapphire mirrors, which are installed at 3-km arm cavity. Members working for KAGRA cryogenic system, which plays an important role for achieving this unique characteristics, are mainly constituted by that of ICRR, KEK, and the University of Toyama. Here, we summarize the activity of members of ICRR in FY 2019.

Cryogenic payload A KAGRA sapphire mirror is suspended by 9-stage suspension and its bottom 4 stages that include sapphire mirror is called cryogenic payload. Angular and translational motion of these sapphire mirrors must be controlled well for operating them as an interferometer. Therefore, damping and global control of suspension were implemented and improved in this fiscal year.

One large improvement of the suspension control is implementation of hierarchical control of suspension. After the implementation of this hierarchical control, angular motion of sapphire mirror became very small: less than 100 nrad in RMS, which is small enough to operate the interferometer. Thanks to this improvement, we succeeded to operate a power-recycling Fabry-Perot Michelson interferometer with the cryogenic payloads.

Heatlink vibration isolation system KAGRA cryogenic payload has heatlinks, which are directly connected to cryocoolers, for cooling sapphire mirror to 20 K. Since cryocooler makes large vibration compared to the ground motion at Kamioka site, the vibration through these heatlinks can be contaminate the detector sensitivity of KAGRA. So, we developed heatlink vibration isolation system (HLVIS) to mitigate the vibration through heatlinks.

HLVIS consists of three-stage pendulum. Each stage is suspended by four tension springs in order to mitigate not only horizontal vibration but also vertical vibration. Vibration isolation ratio was measured below 10 Hz and measurement result was almost matched with designed value.

New design of mirror inclination control system A cryogenic payload has an inclination adjustment system called moving mass system. the moving mass system consists of three components: cryogenic compatible stepper motor, oil-free ball screw, and copper block. We can drive a copper block by rotating stepper motor and change the mass balance of the cryogenic payload to tilt the mirror.

Basically, this moving mass system works well but in terms of long-term stability, there is an issue to be solved. So, we started to re-design the moving mass system. In the new moving mass system, we adopted pulleys instead of ball screw. In FY 2019, an initial design was finished and prototype was fabricated.

Sapphire fiber thermal conductivity In KAGRA cryogenic payload, high purity aluminum heatlink is installed except for the sapphire mirror to cool the suspension effectively. Instead of this, sapphire mirror is cooled only by sapphire fibers in order not to induce additional vibration and mechanical losses to the mirror. So, thermal conductivity of sapphire fibers directly affects the cooling performance of the cryogenic payload.

In FY2019, we measured thermal conductivity of several sapphire samples and obtained 4000 W/m·K at 20 K. This value is slightly lower than KAGRA requirement but we started the collaboration with foreign institute for making better sapphire fibers.

Molecular adosorption at cooled mirror surface Gas molecules that hit to cryogenic objects are trapped at these surface. This effect is called cryopumping effect and its pumping power is very large. So, cryogenic mirror of KAGRA can trap residual gas molecules inside vacuum chamber and make thin layers on the mirror surface. Since the thin layers will change the reflectivity of the mirror, this effect can affect the detector sensitivity of KAGRA. First, we measure the speed of molecular adosorption in the KAGRA cryostat. Then, we calculated the impact for the KAGRA detector sensitivity based on the adosorption speed we measured. In addition to this, we considered the effective way to remove the adsorbed molecules and demonstrated the disorption by using CO_2 laser.

Doctoral theses One doctoral thesis, *Optical and thermal study of molecular thin layers on cryogenic mirrors in next-generation gravitational wave telescopes* was accepted in FY 2019.

Acknowledgement Mechanical workshops of Institute for Solid State Physics (The University of Tokyo, Kashiwa campus) and Mechanical Engineering Center of KEK make a large contribution through providing many products for our research.

Vibration Isolation System Type-A

[Spokesperson : Lucia TROZZO]

ICRR, The Univ. of Tokyo, Hida, Gifu 506-1205 lucia,s contribution

Introduction

Seismic noise gives the most important contribution and it is dominant in the range [0.1,10] Hz. This region is critical for the ground based GW detector, because the seismic noise influence the detector sensitivity and the possibility to operate with high duty cycle: The selection of an experimental site has a key role to limit the impact of seismic noise on interferometric detectors for Gravitational Waves observations. In underground locations the perturbations caused by the atmospheric fluctuation due to the weather conditions are minimal, the environmental conditions are more stable and, as a consequence, the measurable noise on the surface level is attenuated: seismic noise, in the underground facilities, is

about 100 time smaller than those ones on surface: for all these reasons KAGRA has been designed to be underground. Anyway to achieve the target sensitivity of 10^{-18} m/sqrt(Hz) at 10 Hz, suspending optical components is a crucial task in the construction of GW interferometers. In fact the gravitational waves observation depends on the capability to include into the experimental apparatus a free falling mass (test mass), well isolated from all the noise sources which are relevant in the observational frequency band. For these reasons the ground based and broad-band interferometers have been equipped with an appropriate suspension system of the test masses including complex mechanical structures studied to inhibit noise transmission and consider test masses as free-falling from few Hz.

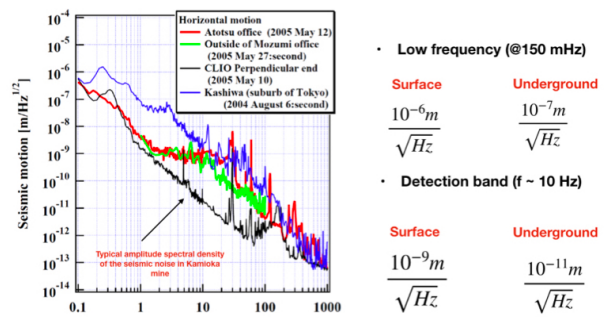


Fig. 10. Seismic noise spectrum on surface in the Tokyo area and the measurements performed at different levels inside the Kamioka mine

Vibration Isolation System for the Cryogenic Mirrors: Type A

A good approximation of a free falling mass is represented by a simple pendulum composed by a thin wire, as elastic element, connected to a body of mass m . Thanks to this simple solution it is possible to filter seismic noise in a real experiment to the optical level by using a harmonic oscillator. In GW detectors seismic isolation with a capability attenuation 10 orders of magnitude is needed: It is evident that a multiple stage pendulum represents a good approach to improve the total attenuation factor of seismic noise at the level of the test masses. Solution adopted in KAGRA is based on the idea to replicate harmonic oscillators of length 2 m to obtain a sophisticated mechanical structure: Type-A suspensions. The Type-A suspension is a nine-stage pendulum with the height of 13.5 m based on the second floor of the underground mine. The top of the suspension has a pre-isolation stage supported by three inverted pendulum legs. The suspension chain consists of cascaded geometric anti-spring filters that show low frequency mechanical resonances. The bottom four stages including the sapphire mirror are called cryogenic payload and cooled down to about 20 K in order to reduce the thermal noises. The whole suspension provide a seismic attenuation of 15 orders of magnitude at 10 Hz.

The suspension system has a negative aspect of amplifying the mirror fluctuation at its resonant frequencies: the excess of the mirror displacement even at an out-of-band frequency disturbs stable operation of the interferometer. We need to

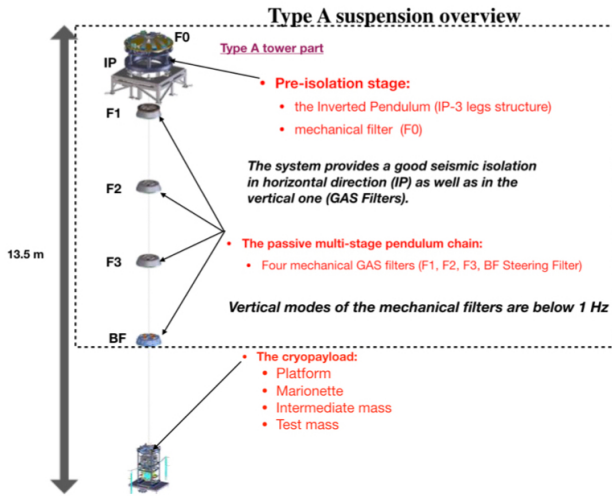


Fig. 11. Drawing of the Type A suspension system

implement damping controls on suspension stage and on the payload, in order reduce the free swinging of the test masses and to make the system robust against external disturbances.

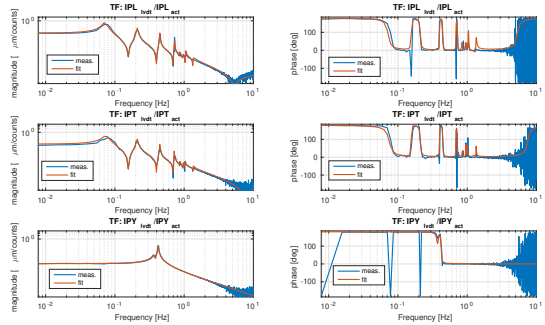


Fig. 12. Normal modes of Type A suspension system

To monitor and control the displacement of the suspension, the system is equipped with several sensors and actuators: position sensors (LVDT), inertial sensors (accelerometer or geophone), photosensors, optical levers, actuators (coil-magnet type). Thanks to the presence of these sensors and actuators a feedback control could be implemented in different points: Inverted Pendulum, vertical GAS filters, Bottom Filter, Marionette stage and the Mirror. The intent of the feedback action is to reduce the swinging of the free falling masses along: -longitudinal, transverse direction by acting on the Top stage (IP); - vertical direction by acting on GAS filters; - angular directions (Pitch and Yaw) by acting on the Bottom Filter, the Marionette and the Intermediate mass stages. At the IP stage the "sensor correction technique" and the "tidal compensation" are also implemented. Thanks to them it is possible to achieve a suppression of microseismic noise, in the range [0.1 0.5] Hz, by about a factor 3 and to compensate for long-term drifts in Fabry-Perot cavities due to the tidal effect, respectively. All these control loops play a crucial role in the locking acquisition process of the whole interferometer:

in fact they are engaged to achieve and to keep its standard working conditions even after a violent unlock event.

Vibration Isolation System Type-B

[Spokesperson : Fabian Peña Arellano]

ICRR, The Univ. of Tokyo, Hida, Gifu 506-1205

Besides the four Type-A suspensions KAGRA relies on smaller suspensions for other mirrors which are always at room temperature. The Type-B suspension is used for the beam splitter and the three signal recycling mirrors, whereas the Type-Bp is used for the three power recycling mirrors.



Fig. 13. The IP of the beam splitter in the vacuum chamber and the installation team.

As in Type-A suspension, in Type-B suspension the first vibration isolation stage is the Inverted Pendulum (IP), whose main goal is to passively attenuate the persistent horizontal microseismic motion produced by ocean activity. Typical resonant frequencies for these IPs are between 60 mHz and 80 mHz in order attenuate the microseismic peak at around 200 mHz. The following three stages, intended for vertical isolation, are three geometric anti-spring filters. The first one lies directly on top of the IP table while the other two hang from it as the masses of a multi-stage pendulum. As in the case of the IP, GAS filters are devices capable of supporting loads of hundreds of kilograms and at the same time achieving resonant frequencies of a few hundreds of millihertz. The horizontal position of the IP and the vertical positions of the GAS filters are measured with Linear Variable Differential Transformers (LVDTs) and are adjusted with coil-magnet actuators which also damp the mechanical resonant motion. The typical resolution of the LVDTs are below 0.2 μm. From the lowermost GAS filter the payload hangs. The payload, which is common to Type-B and Type-Bp suspensions, comprises the optic, its marionette and their respective recoil masses. The recoil mass of the marionette holds local displacement sensors to monitor six degrees of freedom and coil-magnet actuators for damping the resonant modes of oscillation of the suspension itself. The sensors have typical resolutions of about 20 nm. The recoil mass of the mirror holds coil-magnet actuators only and the system relies on an optical lever to monitor the tilt and position of the optic from the ground.

The Type-Bp suspension is shorter and comprises two GAS filters and the payload. The uppermost GAS filter lies directly on the ground while the lowermost one has its own recoil mass in order to attenuate motion which may be excited by the microseismic motion of the ground.

Integrated DAQ/control system using real time computers

[Spokesperson : Shoichi OSHINO]

ICRR, The Univ. of Tokyo, Hida, Gifu 506-1205

The 2019 fiscal year, we started the observation with a power-recycled Fabry-Perot-Michelson interferometer from February 2020. During this observation, we continued to maintain stable DAQ/control system.

Stable operation with the real time control system The first part of 2019 was the process of replacing computers with a faster ones. This is a countermeasure to the glitches that were identified last year, which occur under high loads. Basically the control computers use a real time operating system. Some delay due to the heavy task causes a serious problem for control loops and it emerges as jumps or glitches on many signals. Eventually, by replacing 17 computers, these glitches no longer occur and we are able to control the interferometer with stable digital system.

In the 2018 fiscal year, we used a simple Michelson interferometer to perform operations, but we have to build a more complicated interferometer for the actual observations. Therefore, we have installed various types of hardware to enable more complicated control. In particular, we have installed and enhanced the hardware for length sensing control and output mode cleaner. Finally, we used the digital system of 25 RT-PCs, 50 ADCs, 39 DACs and 73 BIOs to control the interferometer.

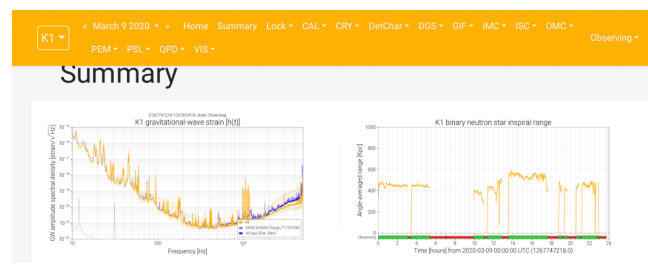
In late 2019, commissioning work of interferometer began and the sensitivity of gravitational wave is visible. Since the DAQ/control system was already stable, we began reducing the noise to improve sensitivity. A number of circuits have been installed in the KAGRA mine. A number of AC-DC converters are also installed to supply power to these circuits. These DC power supplies generate a lot of magnetic noise, which is expected to affect the sensitivity of the interferometer. We solved this problem by replacing the power supplies farther away from the circuit and wiring the power cables. Most of the power supplies have already been replaced. We will continue to replace the remaining power supplies in fiscal year 2020.

Detector Charcterization

[Spokesperson : Takahiro Yamamoto]

ICRR, The Univ. of Tokyo, Hida, Gifu 506-1205

Detector commissioning support The goal of detector characterization is providing the reliable data for gravitational waves searches. In order to achieve this goal, we developed



some data monitor tools such as SummaryPages shown in figure 1. SummaryPage is the web-based data monitor system for supporting detector commissioning activities. Commissioning activities are performed to achieve the stable operation of the interferometer and the target sensitivity. On the gravitational wave observation, more than 100,000 signals are acquired as the observational data. SummaryPage helps us to monitor such a lot of signals efficiently. In addition, since KAGRA joined the international observing network of gravitational waves, SummaryPage also served as an interface for LIGO, Virgo, and KAGRA to know each other's situation.

Observing data validation During the observing run in the end of March 2020, we also provided indicators of the data quality as another major role. These indicators are used to judge whether the data can be used for gravitational wave searches. For the joint gravitational wave search with LIGO and Virgo, we also established to share these data quality indicators.

Physical Environment Monitors

[Spokesperson : Takaaki YOKOZAWA]

ICRR, The Univ. of Tokyo, Hida, Gifu 506-1205

Because the amplitude of gravitational waves(GWs) are very small, we must take care everything which can be a noise source. One of the major noise sources is environmental disturbance through earthquakes, effects from magnetic and acoustic fields, temperature and so on. To investigate the effect from the environmental noise, we installed various types of the monitors, which are called as physical environmental monitors (PEMs). Also, because KAGRA interferometer was developed in the underground environment and operated with cryogenic temperature (20K). Those environment and technique is essential to the next generation GW interferometer. So the understanding of the KAGRA interferometer environment is key technology.

Six seismometers were installed to evaluate the ground motion in the underground environment and those seismometer were also used for the suspension control to reduce the mirror motion. the accelerometers and microphones were also installed to monitor the optical tables. Such auxiliary optics on the optical tables were used for many purpose, such as laser source stabilization, mode matching, sensing for the interferometer control and controls of the photon calibrator. Those PEMs were used for evaluating not only the stationary interferometer noise but also narrow band frequency noise and

transient noise identification.

The temperature monitor is also important for keep the suspensions healthy. If the temperature changed 1 degree, the height of the mirror motion was changed and it became difficult to keep the interferometer condition. For monitoring the temperature, we installed total 77 thermometer, which can monitor both temperature and humidity and made the web site to monitor the temperature drift.

Finally, to evaluate the effect from the environments, we established the system of the environmental injection, such as acoustic injection and magnetic injection system. By performing the acoustic injection, we turned out that the peaks of the 160, 280 and 360 Hz came from the acoustic environmental noise.

Commissioning

[Spokesperson : Osamu MIYAKAWA]

ICRR, The Univ. of Tokyo, Hida, Gifu 506-1205

For KAGRA, it is not an exaggeration to say that the fiscal year of 2019 has been a year of commissioning. By FY2018, almost all of the subsystems had been installed and in FY2019 we targeted to operate as a whole interferometer. We had several engineering runs with the Michelson interferometer, operating in a single arm cavity, and finally carried it through to observation. It is a remarkable result that we were able to achieve the minimum target sensitivity of 1 Mpc. This led to a joint observation with GEO.

In this process, one major problem was exposed: the presence of birefringence in the Sapphire mirror, which was thought to reduce the returning light from the interferometer. This can be a direct problem for sensitivity since the target power-recycling gain cannot be achieved. It was then found that the modal healing effect of the arm cavity relieved this problem and that sufficient power recycling gain could be obtained. However, the sidebands would still be lost due to the birefringence, so we should consider making the mirror again in order to achieve the final sensitivity.

The Fig.14 shows the improvement in sensitivity over a period of about six months. We successfully achieved the first FPMI operation in late August, with both 3 km arms storing light into the arm cavities, and the first sensitivity was measured. At this point, it was found that 4-5 orders of magnitude were necessary to reach the minimum target sensitivity, and we realized that noise-hunting was the most important task for commissioning. We improved the sensitivity initially by resolving a few minor problems. When the sensitivity improvement was a bit slow, the introduction of the ISS (Intensity Stabilization Servo) improved by one order, and the removal of the FSS (Frequency Stabilization Servo) improved by another order of magnitude, total improvement in sensitivity by two orders of magnitude was not insignificant at that time. We continued to try to improve the sensitivity, but since we were using only 10% of the transmitted light of the power recycling mirror, it was difficult to increase the laser power in the interferometer further, which limited the sensitivity at high frequencies.

In January, the PRFPMI which aimed to increase laser power in the interferometer was successfully operated. The laser power could be increased by a factor of 100 compared to the FPMI state. Although there were some concerns about the noise in the control systems, it was found that they did not limit the final sensitivity of the PRFPMI for the observations in 2019, and the operation of PRFPMI was fine. However, we believe that we need to move to DRFPMI to realize the final sensitivity as designed.

The following February we successfully established the OMC (output mode cleaner) in operation. This OMC allowed us to measure the sensitivity of the interferometer using DC power. This is called as a DC readout method that was designed as an final method without using RF sideband signals. The first sensitivity of the DC readout was 40 kpc, which was almost the same as the highest sensitivity of FPMI, and we aimed to improve the sensitivity further. From this point, we improved the sensitivity by one more order of magnitude, and when the sensitivity was about 400 kpc, we started the first observation for two weeks. During the observation, the sensitivity fluctuated several times due to uncertainties of calibration. This issue is still under investigation, and further verification is necessary. Finally, we achieved the minimum target sensitivity of 1 Mpc, and this led to the second round of observations in April.

Through this commissioning, it was found that both sensitivity and stability are highly dependent on the alignment of mirrors. The angular control of the mirror has been successfully introduced in some degrees of freedom. In order to achieve the final sensitivity, it is necessary to introduce the angular control for all the degrees of freedom. It was also exposed that weakness for climate change, such as micro seismic motion in the 0.1 Hz band existed. This needs to be resolved by improving the control system of the vibration isolation system.

There were various problems and issues during the commissioning process, and most of them were solved and the stable operation was achieved. Although, there are still some problems to be solved, but it is remarkable that we have established the 4-5 orders of magnitude improvement of the sensitivity in only 6 months. In the future, we will update the vibration isolation system and try to achieve the final target sensitivity through further commissioning.

Observation

[Spokesperson : Shinji MIYOKI]

ICRR, The Univ. of Tokyo, Hida, Gifu 506-1205

After the commissioning as referred in the previous paragraph, KAGRA has finally started its GW observation from 25th February to March 7th with 250 kpc ~ 500 kpc binary range sensitivity for GWs from BNS mergers. After that, another GW network observation with GEO600 gravitational wave telescope was done from 7th April to 21st April with about 500 kpc ~ 800kpc sensitivity. Between these two observations, an additional commissioning was performed to enhance its sensitivity and stability as a telescope. Finally, KAGRA sensitivity reached around 1 Mpc that was

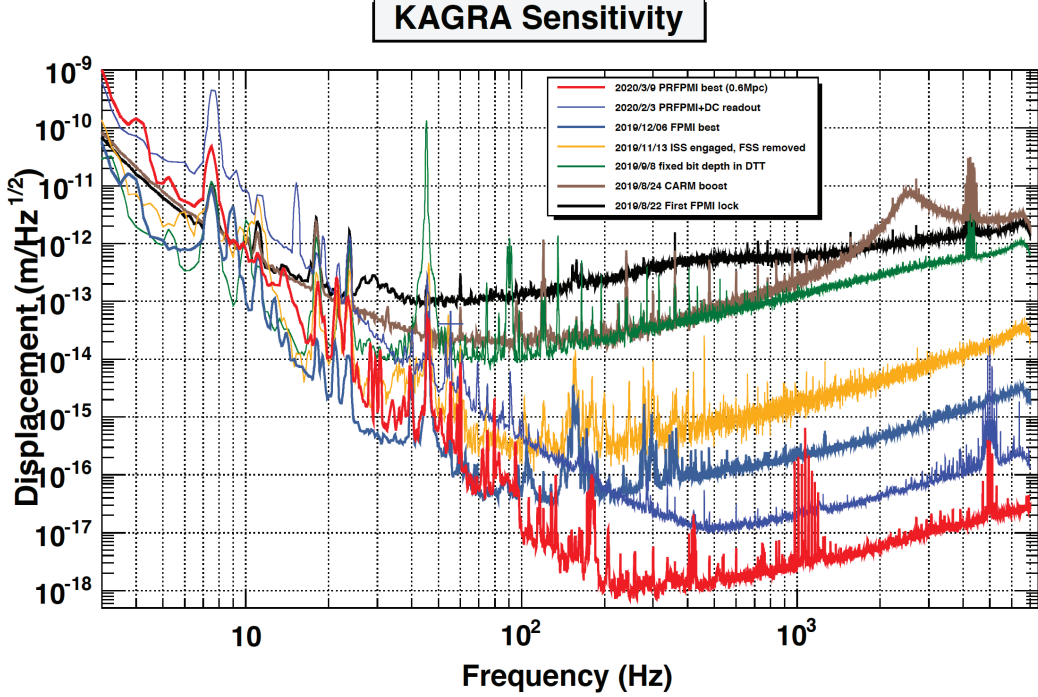


Fig. 14. Improvement of the KAGRA sensitivity in 6 months.

one of criteria for KAGRA to join the GW observation network with Adv.LIGO, Adv.Virgo and GEO600. In order to participate in this international GW observation network with Adv.LIGO, Adv.Virgo and GEO600, not only the sensitivity around 1 Mpc binary range, but also many requested criteria were cleared. They are (1) calibration of time domain strain sensitivity, $h(t)$, and its uncertainty budget, (2) preparation of state vector information, (3) rapid response team formation, (4) low-latency KAGRA data transfer to CIT/Virgo, (5) collaboration general computing support, (6) data quality segment database preparation, (7) webpage for IFO status monitor and (8) high-latency data transfer between KAGRA and LV from the October 2019. The latter observation was regarded as “O3GK” that were performed according to the LVK MOA that was made in October in 2019. During O3GK, However, Adv.LIGO and Adv.Virgo were offline because of COVID-19 problems. Both observations had engineering runs for a week just before each observation for mainly calibration. Calibration was also done just after observations to evaluate the error range of KAGRA sensitivity. Each observation was operated in three shift system by one operator and one co-operator those were supported by expert members for operational emergency. The duty cycle for O3GK was 53.2% in science mode and 58.8% in locked mode. During the online state of both KAGRA and GEO600 during O3GK, an astronomical gamma-ray burst event named “GRB200415A” was reported. We are now analyzing our data on this event.

Data Analysis

[Spokesperson : Hideyuki Tagoshi]

ICRR, The Univ. of Tokyo, Kashiwa, Chiba, 277-8582

There are variety of data related activities in KAGRA. The main data server of KAGRA is located at ICRR Kashiwa. It has a 2.5PiB data storage. All KAGRA data taken at Kamioka are packed into one file for every 32 seconds, and are transferred continuously to the main data server at Kashiwa. Beside this, low latency data transfer is also done by packing only main interferometer data into one file for every 1 seconds. For low latency data transfer, the latency of about 3 seconds is achieved from Kamioka to Kashiwa (this time include the time necessary for calibration).

KAGRA detector is producing several hundreds thousands of channels of data which record signals from various sensors, signals to control instruments, signals to monitor environment of the detector. Those data are used to check the status of detector and to improve the sensitivity. It is important to introduce convenient tools to visualize the data in order to accelerate the installation and commissioning works. Web based visualization tools are now being developed. Some of tools developed by LIGO group are also installed. These tools are also useful when gravitational wave signals are detected. In order to have a confidence of detection of gravitational wave signals, it is important to investigate environmental channels whether there are any noise sources which might produce data which are similar to real gravitational wave signals. These visualization tools can be used to check various environmental channel data.

In order to detect gravitational wave signals, several pipelines have been developed in KAGRA. Among them, a pipeline to search for gravitational waves from compact binary coalescences (CBC) are developed in KAGRA Algorith-

mic Library (KAGALI). KAGALI is a common data analysis library written mainly in C. The CBC pipeline have been used to analyze KAGRA data during iKAGRA operation. Improvement of the CBC pipeline are now ongoing in order to treat multiple detectors and to introduce the spin parameters in the waveform. These tasks will be continued in 2019. The improvement of the parameter estimation pipeline for CBC signals based on the Markov Chain Monte Carlo method was continued from the last year. This work is lead by Hyung Won Lee (Inje Univ).

There are several efforts to introduce new data analysis methods in the analysis of gravitational wave data. Among them, the performance of Non-Harmonic Analysis (NHA) in visualizing the time-frequency behavior of the data was evaluated. NHA is a method to evaluate the spectrum of data by evaluating multiple instantaneous frequencies and amplitudes of data in a way which is different from discrete Fourier transform. We find that there are various advantage in NHA in visualizing CBC signals compared with the method of short time Fourier transform. We apply NHA to public data of LIGO-Virgo events, like GW150914, GW170817, and demonstrated the visualization of the signal on time-frequency plane. This work has been done in collaboration with the group of Shigeki Hirobayashi (Univ. Toyama).

Ref. Kenta Yanagisawa , Dongbao Jia, Shigeki Hirobayashi, Nami Uchikata , Tatsuya Narikawa, Koh Ueno, Hirotaka Takahashi, Hideyuki Tagoshi, PTEP 2019 (2019) no.6, 063F01.

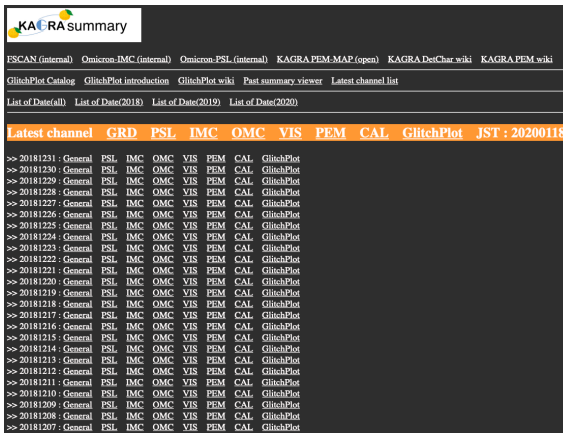


Fig. 15. Example of summary page

Bibliography

- [1] S. Ueda, K. Somiya et al., Class. Quantum Grav. 31 095003 (2014)
- [2] K Yamamoto et al., Class. Quantum Grav. 36 (2019) 205009.

Observational Cosmology Group

[Spokesperson : Yoshiaki Ono]

ICRR, The Univ. of Tokyo, Kashiwa, Chiba 277-8582

SILVERRUSH. VIII. Spectroscopic Identifications of Early Large-scale Structures with Protoclusters over 200 Mpc at $z \sim 6-7$: Strong Associations of Dusty Star-forming Galaxies [1]

In collaboration with the members of The University of Tokyo, National Astronomical Observatory of Japan, Aix Marseille University, Kitami Institute of Technology, California Institute of Technology, National Tsing Hua University, Osaka Sangyo University, Academia Sinica, University of California, Santa Barbara, Observatorio Nacional, Universidade de Sao Paulo, Durham University, RIKEN, Purple Mountain Observatory, Dalhousie University, Imperial College London, Seoul National University, Shanghai Jiao Tong University, Onomichi City University, Subaru Telescope, Nagoya University, Ehime University, and Cosmic Dawn Center.

We have obtained three-dimensional maps of the universe in $\sim 200 \times 200 \times 80$ comoving Mpc³ (cMpc³) volumes each at $z = 5.7$ and 6.6 based on a spectroscopic sample of 179 galaxies that achieves $\gtrsim 80\%$ completeness down to the Ly α luminosity of $\log(L_{Ly\alpha}/[\text{erg s}^{-1}]) = 43.0$, based on our Keck and Gemini observations and the literature (Figure 16). The maps reveal filamentary large-scale structures and two remarkable overdensities made out of at least 44 and 12 galaxies at $z = 5.692$ (z57OD) and $z = 6.585$ (z66OD), respectively, making z66OD the most distant overdensity spectroscopically confirmed to date, with > 10 spectroscopically confirmed galaxies. We compare spatial distributions of submillimeter galaxies at $z \simeq 4 - 6$ with our $z = 5.7$ galaxies forming the large-scale structures, and detect a 99.97% signal of cross-correlation, indicative of a clear coincidence of dusty star-forming galaxy and dust-unobscured galaxy formation at this early epoch. The galaxies in z57OD and z66OD are actively forming stars with star-formation rates (SFRs) $\gtrsim 5$ times higher than the main sequence, and particularly the SFR density (SFRD) in z57OD is 10 times higher than the cosmic average at the redshift (a.k.a. the Madau-Lilly plot). Comparisons with numerical simulations suggest that z57OD and z66OD are protoclusters that are progenitors of the present-day clusters with halo masses of $\sim 10^{14} M_\odot$.

Bibliography

- [1] Harikane, Y., Ouchi, M., Ono, Y., Fujimoto, S., Donevski, D., Shibuya, T., Faisst, A. L., Goto, T., Hatsukade, B., Kashikawa, N., Kohno, K., Hashimoto, T., Higuchi, R., Inoue, A. K., Lin, Y.-T., Martin, C. L., Overzier, R., Smail, I., Toshikawa, J., Umehata, H., Ao, Y., Chapman, S., Clements, D. L., Im, M., Jing, Y., Kawaguchi, T., Lee, C.-H., Lee, M. M., Lin, L., Matsuoka, Y., Marinello, M., Nagao, T., Onodera, M., Toft, S., Wang, W.-H. 2019, The Astrophysical Journal, 883, 142

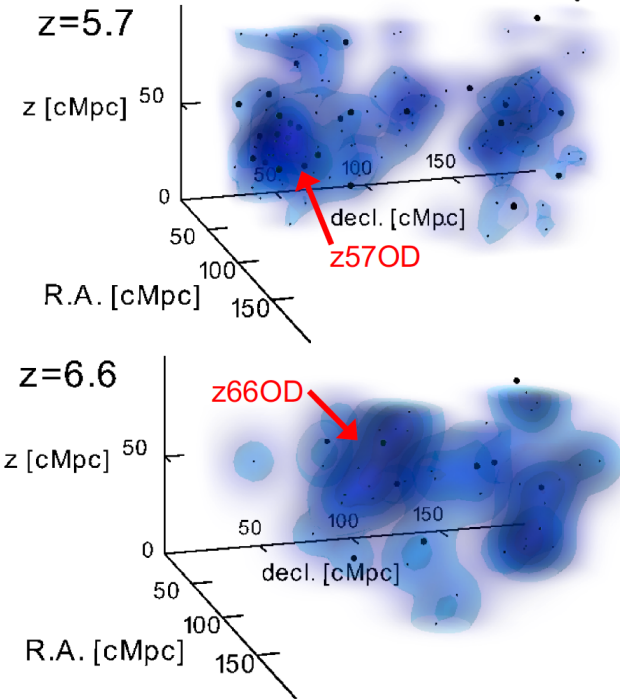


Fig. 16. 3D overdensity maps of Ly α emitters (LAEs) at $z = 5.7$ (top) and $z = 6.6$ (bottom). The black dots show the positions of the LAEs. The large dots are LAEs brighter than $L_{\text{Ly}\alpha} > 10^{43}$ erg s $^{-1}$. Higher density regions are indicated by the bluer colors, smoothed with a Gaussian kernel of $\sigma = 10$ cMpc (15 cMpc) at $z = 5.7$ ($z = 6.6$).

Fast Outflows Identified in Early Star-forming Galaxies at $z = 5\text{--}6$ [2]

In collaboration with the members of The University of Tokyo, National Astronomical Observatory of Japan, The University of Lyon, and Leiden Observatory.

We present velocities of galactic outflows in seven star-forming galaxies at $z = 5\text{--}6$ with stellar masses of $M_* \sim 10^{10.1} M_\odot$. Although it is challenging to observationally determine the outflow velocities, we overcome this by using Atacama Large Millimeter/submillimeter Array (ALMA) [CII]158 μm emission lines for systemic velocities and deep Keck spectra with metal absorption lines for velocity profiles available to date. We construct a composite Keck spectrum of the galaxies at $z = 5\text{--}6$ with the [CII]-systemic velocities, and fit outflow-line profiles to the SiIII $\lambda 1260$, CII $\lambda 1335$, and SiIV $\lambda\lambda 1394, 1403$ absorption lines in the composite spectrum. We measure the maximum (90%) and central outflow velocities to be $v_{\text{max}} = 700_{-110}^{+180}$ km s $^{-1}$ and $v_{\text{out}} = 400_{-150}^{+100}$ km s $^{-1}$ on average, respectively, showing no significant differences between the outflow velocities derived with the low-to high-ionization absorption lines. For $M_* \sim 10^{10.1} M_\odot$, we find that the v_{max} value of our $z = 5\text{--}6$ galaxies is 3 times higher than those of $z \sim 0$ galaxies and comparable to $z \sim 2$ galaxies. Estimating the halo circular velocity v_{cir} from the stellar masses and the abundance matching results, we investigate a $v_{\text{max}}\text{-}v_{\text{cir}}$ relation (Figure 17). Interestingly, v_{max} for galaxies with $M_* = 10^{10.0\text{--}10.8} M_\odot$ shows a clear positive correlation with v_{cir} and/or the galaxy star formation rate over

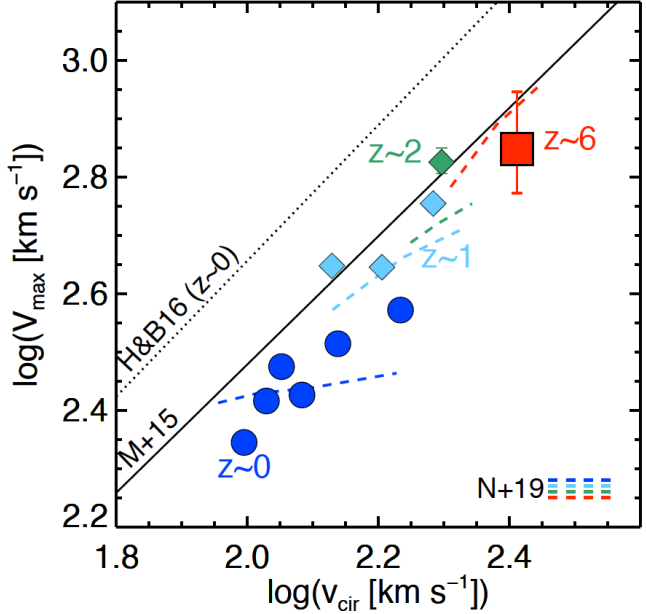


Fig. 17. v_{max} as a function of the circular velocity v_{cir} that are converted from the stellar mass. The filled red square indicates our results at $z = 5\text{--}6$ measured with the simultaneous fitting of the SiIII and CII lines. The data points at $z \sim 0$ (blue) and $z \sim 1$ (cyan) are taken from our previous work. The data point at $z \sim 2$ is derived from the composite spectrum in our previous work, but re-calculated in the manner of this work. The solid black line and colored dashed lines are obtained in the literature. The solid black line and colored dashed lines represent a theoretical relation at $z = 0.5\text{--}4$ predicted by the FIRE simulations (the flux-weighted average 90th percentile velocity) and relations at $z = 0$ (blue), 1 (cyan), 2 (green), and 6 (red) predicted by the IllustrisTNG simulation (90th percentile velocity), respectively. The dotted line indicates a relation of extreme-starburst galaxies $z \sim 0$.

$z = 0\text{--}6$ with a small scatter of $\simeq \pm 0.1$ dex, which is in good agreement with theoretical predictions. This positive correlation suggests that the outflow velocity is physically related to the halo circular velocity, and that the redshift evolution of v_{max} at fixed M_* is explained by the increase in v_{cir} toward high redshift.

Bibliography

- [2] Sugahara, Y., Ouchi, M., Harikane, Y., Bouché, N., Mitchell, P. D., Blaizot, J. 2019, The Astrophysical Journal, 886, 29

First Identification of 10 kpc [CII] 158 μm Halos around Star-forming Galaxies at $z = 5\text{--}7$ [3]

In collaboration with the members of The University of Tokyo, National Astronomical Observatory of Japan, Waseda University, Scuola Normale Superiore, Centro Fermi, European Southern Observatory, University of Edinburgh, Osaka University, University of Tsukuba, and University of Nevada.

We report the discovery of 10 kpc [CII] 158 μm halos surrounding star-forming galaxies in the early Universe. We choose deep ALMA data of 18 galaxies, each with a star-formation rate of $\simeq 10\text{--}70 M_\odot \text{ yr}^{-1}$ with no signature of active

galactic nucleus (AGN) whose [CII] lines are individually detected at $z = 5.153\text{--}7.142$, and we conduct stacking of the [CII] lines and dust continuum in the *uv*-visibility plane. The radial profiles of the surface brightnesses show a 10 kpc scale [CII] halo at the 9.2σ level, significantly more extended than the *Hubble Space Telescope* (HST) stellar continuum data by a factor of ~ 5 on the exponential-profile basis, as well as the dust continuum (Figure 18). We compare the radial profiles of [CII] and Ly α halos universally found in star-forming galaxies at this epoch, and find that the scale lengths agree within 1σ level. While two independent hydrodynamic zoom-in simulations match the dust and stellar continuum properties, the simulations cannot reproduce the extended [CII] line emission. The existence of the extended [CII] halo is evidence of outflow remnants in the early galaxies and suggests that the outflows may be dominated by cold-mode outflows expelling the neutral gas.

Bibliography

- [3] Fujimoto, S., Ouchi, M., Ferrara, A., Pallottini, A., Ivison, R. J., Behrens, C., Gallerani, S., Arata, S., Yajima, H., Nagamine, K. 2019, The Astrophysical Journal, 887, 107

Balmer Break Galaxy Candidates at $z \sim 6$: A Potential View on the Star Formation Activity at $z \gtrsim 14$ [4]

In collaboration with the members of Osaka Sangyo University, Waseda University, National Astronomical Observatory of Japan, University of Tsukuba, The University of Tokyo, Ehime University, Japan Aerospace Exploration Agency, Tohoku University, California Institute of Technology, Academia Sinica, and The Open University of Japan.

We search for galaxies with a strong Balmer break (Balmer Break Galaxies; BBGs) at $z \sim 6$ over a 0.41 deg^2 effective area in the COSMOS field. Based on rich imaging data, including data obtained with the ALMA, three candidates are identified by their extremely red $K - [3.6]$ colors, as well as by non-detection in X-ray, optical, FIR, and radio bands. The non-detection in the deep ALMA observations suggests that they are not dusty galaxies but BBGs at $z \sim 6$, although contamination from AGNs at $z \sim 0$ cannot be completely ruled out for the moment. Our spectral energy distribution (SED) analyses reveal that the BBG candidates at $z \sim 6$ have stellar masses of $\approx 5 \times 10^{10} M_\odot$ dominated by old stellar populations with ages of $\gtrsim 700$ Myr. Assuming that all the three candidates are real BBGs at $z \sim 6$, we estimate the stellar mass density (SMD) to be $2.4_{-1.3}^{+2.3} \times 10^4 M_\odot \text{ Mpc}^{-3}$ (Figure 19). This is consistent with an extrapolation from the lower-redshift measurements. The onset of star formation in the three BBG candidates is expected to be several hundred million years before the observed epoch of $z \sim 6$. We estimate the SFRD contributed by progenitors of the BBGs to be $(2.4\text{--}12) \times 10^{-5} M_\odot \text{ yr}^{-1} \text{ Mpc}^{-3}$ at $z > 14$ (99.7% confidence range). Our result suggests a smooth evolution of the SFRD beyond $z = 8$.

Bibliography

- [4] Mawatari, K., Inoue, A. K., Hashimoto, T., Silverman, J., Kajisawa, M., Yamanaka, S., Yamada, T., Davidzon, I., Capak, P., Lin, L., Hsieh, B.-C., Taniguchi, Y., Tanaka, M., Ono, Y., Harikane, Y., Sugahara, Y., Fujimoto, S., Nagao, T. 2020, The Astrophysical Journal, 889, 137

CHORUS. III. Photometric and Spectroscopic Properties of Ly α Blobs at $z = 4.9\text{--}7.0$ [5]

In collaboration with the members of The University of Tokyo, Kitami Institute of Technology, National Astronomical Observatory of Japan, Osaka Sangyo University, Waseda University, The Observatories of the Carnegie Institution for Science, University of Tsukuba, Osaka University, The Graduate University for Advanced Studies, Kure College, Observatoire de Geneve, Ehime University, and The Open University of Japan.

We report the Subaru Hyper Suprime-Cam (HSC) discovery of two Ly α blobs (LABs), dubbed z70-1 and z49-1 at $z = 6.965$ and $z = 4.888$ respectively, that are Ly α emitters with a bright ($\log L_{\text{Ly}\alpha}/[\text{erg s}^{-1}] > 43.4$) and spatially-extended Ly α emission, and present the photometric and spectroscopic properties of a total of seven LABs: the two new LABs and five previously known LABs at $z = 5.7\text{--}6.6$. The z70-1 LAB shows extended Ly α emission with a scale length of 1.4 ± 0.2 kpc, about three times larger than the UV continuum emission, making z70-1 the most distant LAB identified to date. All of the seven LABs, except z49-1, exhibit no AGN signatures such as X-ray emission, N $\lambda 1240$ emission, or Ly α line broadening, while z49-1 has a strong C $\lambda 1548$ emission line indicating an AGN on the basis of the UV-line ratio diagnostics. We carefully model the point-spread functions of the HSC images and conduct two-component exponential profile fitting to the extended Ly α emission of the LABs. The Ly α scale lengths of the core (star-forming region) and halo components are $r_c = 0.6\text{--}1.2$ kpc and $r_h = 2.0\text{--}13.8$ kpc, respectively. The relations between the scale lengths and galaxy properties (Ly α luminosity $L_{\text{Ly}\alpha}$, Ly α rest-frame equivalent width EW_0 , and UV continuum magnitude M_{UV}) of our LABs are similar to those of Ly α halos (LAHs) identified around star-forming galaxies found previously by VLT/MUSE at similar redshifts (Figure 20), suggesting that our LABs are likely the bright version of high- z LAHs.

Bibliography

- [5] Zhang, H., Ouchi, M., Itoh, R., Shibuya, T., Ono, Y., Harikane, Y., Inoue, A. K., Rauch, M., Kikuchihihara, S., Nakajima, K., Yajima, H., Arata, S., Abe, M., Iwata, I., Kashikawa, N., Kawanomoto, S., Kikuta, S., Kobayashi, M., Kusakabe, H., Mawatari, K., Nagao, T., Shimasaku, K., Taniguchi, Y. 2020, The Astrophysical Journal, 891, 177

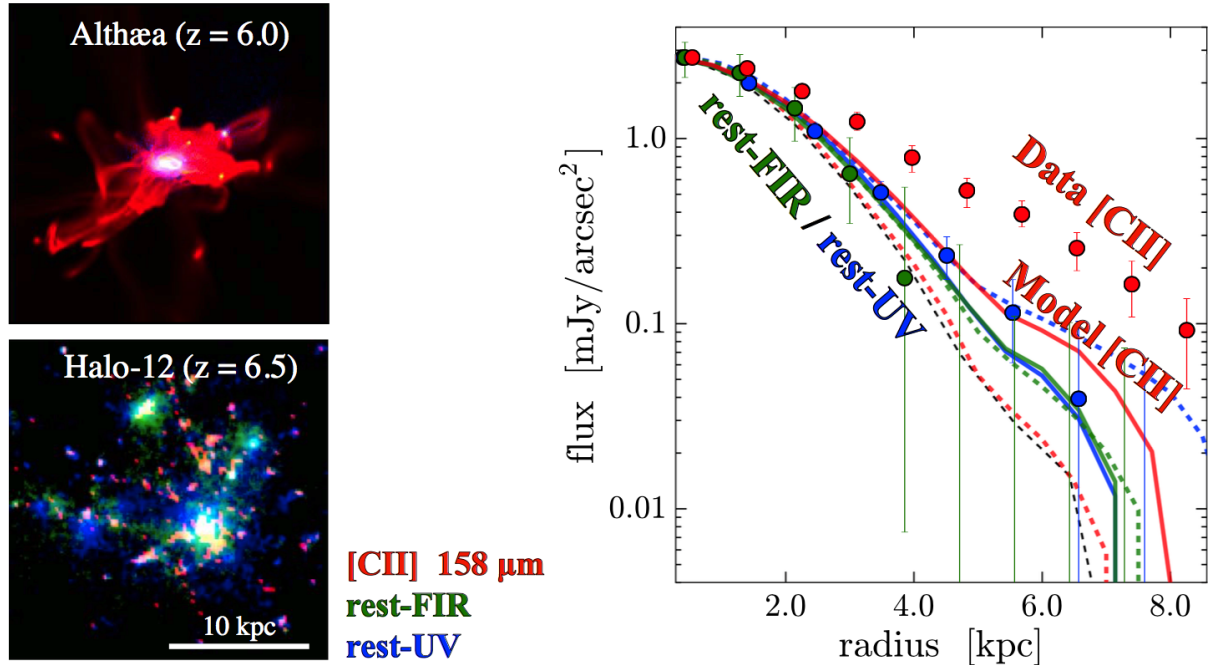


Fig. 18. **Left:** $4'' \times 4''$ fake-color image for Althaea at $z = 6.0$ (top) and Halo-12 (bottom) in the zoom-in simulations (red: [CII] line, green: rest-frame far-infrared (FIR) continuum, blue: rest-frame UV continuum). **Right:** radial surface brightness profiles of the [CII] line (red curve), rest-frame FIR (green curve), and UV (blue curve) continuum emission estimated in the zoom-in simulations via a stacking procedure. The solid and dashed color lines represent the Althaea and Halo-12 results, respectively. The black dashed curve denotes the ALMA synthesized beam. The circles indicate the ALMA-HST stacking results, whose colors are assigned in the same manner as the left panel.

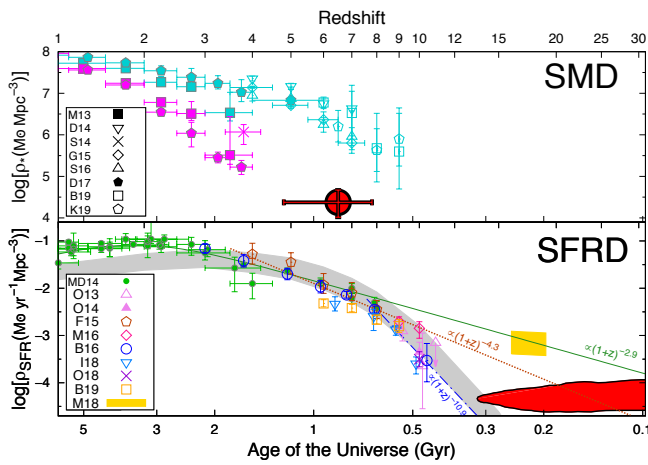


Fig. 19. Evolution of the SMD (top) and the SFRD (bottom) along the cosmic history (see top axis for the corresponding redshift). For these plots, we assume all the three BBG candidates without ALMA detection to be real passive galaxies at $z \sim 6$. In the top panel, the SMD of our BBG sample at $z \sim 6$ (red circle) is shown in conjunction with those of star-forming (cyan symbols) and passive (magenta symbols) galaxies at lower redshifts from the literature. The vertical error bar associated with our BBG data corresponds to a 1σ uncertainty propagated from the Poisson error for the BBG number and the SED fitting uncertainty for the stellar mass. The horizontal error bar shows the redshift range expected from our BBG color selection. In the bottom panel, the red shaded region corresponds to the SFRD expected from the progenitors of the $z \sim 6$ BBGs at a 99.7% confidence level (3σ). The SFRD measurements at $z \lesssim 10$ are collected from the literature. All of them at $4 \lesssim z \lesssim 10$ are estimated by integrating the UV luminosity functions down to $M_{\text{UV}} = -17$ mag. The SFRD estimated at $z \sim 17$ from an observed global 21 cm absorption trough is also shown in yellow. The functional fit to the MD14 data, which is proportional to $(1+z)^{-2.9}$ at high- z , is superposed by the solid line. Two other power-law functions supporting an accelerated evolution at $z \gtrsim 8$ ($\rho_{\text{SFR}} \propto (1+z)^{-10.9}$) and a smooth evolution from lower redshift ($\rho_{\text{SFR}} \propto (1+z)^{-4.3}$) are shown by dotted-dashed and dotted lines, respectively. The SFRD derived assuming a universal relation among the halo mass, SFR, and dark matter accretion rate is also superposed by the gray shade in its 1σ uncertainty. All of the SMD and SFRD measurements from the literature are corrected for the stellar IMF and the cosmological model to match those in this work.

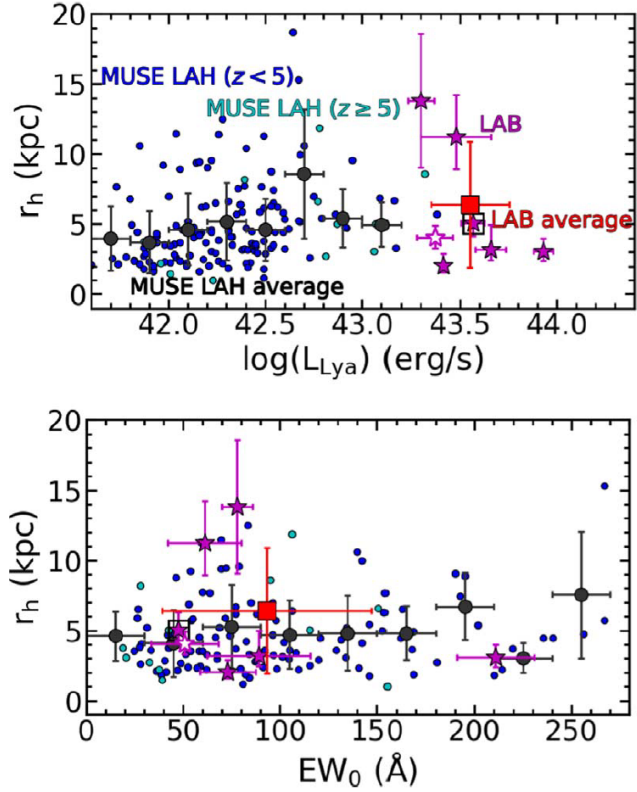


Fig. 20. Halo scale length as a function of Ly α luminosity (top) and Ly α rest-frame equivalent width (bottom) of the seven LABs (stars) and LAHs (filled circles) from the literature. The empty star represents z57-2, which does not have a two-component fitting result. The red filled square shows the average value of our LABs, with error bars indicating the rms. The MUSE LAHs at $z < 5$ and $z \geq 5$ are the blue and cyan filled circles, respectively. The average values of the MUSE LAHs are shown as black filled circles. The black horizontal error bar indicates the bin size, while the black vertical error bar is the rms. In the top panel, we slightly shift z49-1 (boxed star) along the horizontal axis by +0.03 to avoid overlaps.

KAGRA OBSERVATORY

KAGRA observatory is located in the Ikenoyama-mountain on the border between Gifu and Toyama prefecture, about 35 km south of Toyama city in Japan. The observatory was established in 2016 in order to operate Large -scale Cryogenic Gravitational Wave Telescope (nicknamed “KAGRA”). KAGRA itself has a L-shape tunnel facility, and it is located more than 200m under Mt.Ikeno-yama. The corner station of the L-shape tunnel is accessible through a 500-m horizontal access tunnel from Atotsu area. The observatory has its own surface research buildings and rental space in the community center of Hida city located about 5km away from the Atotsu entrance of KAGRA.

KAGRA aims to observe several gravitational waves (GWs) per a year with its designed sensitivity as one of observatories of the world GW detection network including Advanced-LIGO, Advanced-Virgo and planned LIGO-India. KAGRA project (formerly named LCGT) was partially approved in 2010 as one of Leading-edge Research Infrastructure Program, and also supported by Program for Promoting Large-scale Science Projects, Subsidy for Facilities Expense and Grants-in-Aid for Scientific Research from Ministry of

Education, Culture, Sports, Science and Technology (MEXT).

In the KAGRA project, Institute for Cosmic Ray Research plays a role of a host promoting institute, and National Astronomical Observatory in Japan (NAOJ) and High Energy Accelerator Research Organization (KEK) are the main support organizations, then more than 297 researchers in 85 institutes and universities in the world are collaborating for construction and data analysis of KAGRA.

The tunnel excavation started in May 2012, and finished in March 2014. After that, the basic laboratory environment was prepared until September 2015. A Michelson interferometer with 3km arm (iKAGRA) was demonstrated in March 2016, and the first engineering run was performed until May 2016. In 2019, all the interferometer components had been installed to complete the KAGRA Observatory that adopts a power recycled Fabry-Perot Michelson type interferometer with the resonant sideband extraction. On February 25th, 2020, KAGRA started its first observation run. After performing the observation until April 2020, KAGRA will be upgraded and prepared for the joint observation with LIGO and Virgo which is expected to start in the end of 2021.



Fig. 1. Surface Research Building.



Fig. 2. Atotsu Entrance of KAGRA.